Conference on Modelling Fluid Flow (CMFF'15)
The 16th International Conference on Fluid Flow Technologies
Budapest, Hungary, September 1-4, 2015

TWO-PARAMETER BIFURCATION ANALYSIS FOR THE SEEKING OF HIGH AMPLITUDE OSCILLATION OF A PERIODICALLY DRIVEN GAS BUBBLE IN GLYCERINE

Kálmán KLAPCSIK[1], Ferenc HEGEDŰS[2]

[1] Corresponding Author. Department of Hydrodynamic Systems, Budapest University of Technology and Economics. P.O. Box 91, 1521 Budapest, Hungary. Tel.: +36 1 463 1680, Fax: +36 1 463 3091, E-mail: kklapcsik@hds.bme.hu
[2] Department of Hydrodynamic Systems, Budapest University of Technology and Economics. E-mail: hegedusf@hds.bme.hu

ABSTRACT

The dynamics of a harmonically driven spherical gas/vapour bubble has been studied intensely in the last decades. The collapse of a bubble induce extreme conditions, such as high pressure and temperature or even shock waves. The ultrasonic technology exploit these conditions in various fields of industry, for example, ultrasonic pasteurization, alteration of the viscosity of thixotropic fluids, production of new kind of copolymers, or in cancer therapy. The present study intends to aid the applications through the numerical investigation of a harmonically excited spherical gas bubble placed in the highly viscous glycerine. We seek parameter regions where the bubble wall velocities as high as possible, perhaps even higher than the sound speed in the liquid domain. Such kind of high amplitude, collapse-like radial oscillations are difficult to find due to the very high viscosity, which is approximately three orders of magnitude greater than of water. The two investigated parameters were the pressure amplitude and the frequency of the harmonic forcing. The applied model was the Keller—Miksis equation, which is a second order nonlinear ordinary differential equation, describing the bubble wall motion and taking into account liquid compressibility as a first order approximation.

Keywords: Bubble dynamics, bifurcation structure, non-linear analysis, Keller-Miksis equation, glycerine, chaos

NOMENCLATURE

M	[-]	Mach number
P_∞	[bar]	ambient pressure
R	[mm]	bubble radius
R_0	[mm]	reference bubble radius
R_E	[mm]	equilibrium radius
$\dot{R}$	[m/s]	bubble wall velocity
$\ddot{R}$	[m/s^2]	bubble wall acceleration
T_∞	[$°C$]	ambient temperature
c	[m/s]	sound velocity
f	[Hz]	frequency of the bubble oscillation
f_0	[Hz]	linear eigenfrequency of the undamped bubble oscillation
m_G	[g]	mass of the gas inside the bubble
p_{G0}	[Pa]	reference gas pressure
p	[Pa]	pressure
p_A	[bar]	pressure amplitude
p_∞	[bar]	pressure away from bubble
t	[s]	time
t_0	[s]	period of driving time
κ	[-]	ratio of specific heats
μ	[$Pa{\cdot}s$]	dynamic viscosity
ν	[Hz]	driving frequency
ρ	[kg/m^3]	density
σ	[N/m]	surface tension
τ	[-]	dimensionless time
τ_0	[-]	dimensionless period of driving
ω	[rad/s]	angular frequency of excitation
ω_0	[rad/s]	linear angular eigenfrequency of undamped system
ω_R	[-]	relative frequency

Subscripts and Superscripts

G, L, V	gas, liquid, vapour
Max	maximal
ref	reference quantity

1. INTRODUCTION

Cavitation causes serious damage in common engineering application, such as in turbomachinery and in hydraulic systems. In most cases, cavitation occurs as sheet cavitation or bubble swarm, thus the applicability of numerical results on a single

spherical bubble is limited. However, there are special applications in which the spherical geometry is a proper assumption, such as in case of microbubbles [1], since the surface tension contract the bubble as small and as spherical as possible.

Although the spherical geometry is rather simple, the dynamics of the bubble can be very complicated. The excited bubble behave as an oscillatory system. During its oscillation, the bubble wall velocity can be extremely high due to the inertia of the liquid domain, resulting in many orders of magnitude smaller bubble size than the equilibrium state. This process is called as collapse phase. At the minimum bubble radius, the pressure and the temperature can reach 1000 *bar* and 8000 *K* [2]. Due to the high temperature, chemical reactions can take place, producing free radicals such as H', H_2, O', OH', HO_2' HO', H_2O_2, [3, 4], which are the keen interest of a special field of chemistry, called sonochemistry. Taleyarkhan et al. [5] and Lahey et al. [6] observe neutron emission in deuterated acetone, indicating the presence of fusion. Taleyarkhan et al. [5] numerically revealed that the temperature inside a highly compressed bubble can reach 10^6 to 10^7 *K*, supporting the experimental observation.

In the last decades, many industrial applications, related to the ultrasonic technology, have emerged. The main aim is to enhance the mass, heat and momentum transfer between various phases by exploiting the physical effects of the collapse of gas/vapour bubbles. For instance, a promising process in food preservation is the ultrasonic pasteurization. At moderate temperature, approximately at 50 *°C*, the membrane of the bacterial weakens and become less resistant against cavitation damage. Knorr et al. [7] successfully reduce the amount of E. Coli bacteria in whole eggs. Ultrasound used widely in polymer research. A number of studies reported that, the molecular weight and the chain length can be reduced during high intensity ultrasound irradiation [8]. The ultrasonic technology can be used in cancer therapy as well [9-11]. The collapse of the bubble damage the solid tumours aiding the transport of genes and medicines through the cell.

The main motivation to support the applications through the numerical investigation of a harmonically excited spherical gas bubble placed in the highly viscous glycerine. We seek parameter regions where the bubble wall velocities as high as possible, even higher than the sound speed in the liquid domain. The viscosity of the glycerine is approximately three times larger than that of water, therefore the system has a high damping effect, which makes the hunting for high amplitude collapse-like bubble oscillation difficult. The applied bubble model is the Keller—Miksis equation [12], which is a second order nonlinear ordinary differential equation describing the bubble wall motion and taking into account liquid compressibility as a first order approximation. According to the ultrasonic technology, the two investigated parameters are the pressure amplitude p_A and the frequency ν of the harmonic excitation.

2. MATHEMATICAL MODEL

During the numerical investigation, the well-known Keller—Miksis equation was used with some minor modification according to Lauterborn and Kurz [13]:

$$\left(1-\frac{\dot{R}}{c_L}\right)R\ddot{R}+\left(1-\frac{\dot{R}}{3c_L}\right)\frac{3}{2}\dot{R}^2=\left(1+\frac{\dot{R}}{c_L}+\frac{R}{\rho_L c_L}\frac{d}{dt}\right)\frac{(p_L-p_\infty)}{\rho_L}. \quad (1)$$

It is a second order, nonlinear ordinary differential equation describing the variation of the bubble radius $R(t)$ in time, where c_L sound velocity in the liquid domain, ρ_L liquid density, p_L pressure at the bubble wall. The material properties depend on the ambient temperature T_∞ of the liquid domain. The pressure far away from the bubble $p_\infty(t)$ consist of a static and a periodic component, according to the ultrasonic irradiation:

$$p_\infty(t)=P_\infty+p_A\cdot sin(\omega t), \quad (2)$$

there P_∞ is the ambient pressure in the liquid domain, p_A and $\omega=2\pi\nu$ are the pressure amplitude and angular frequency of the harmonic excitation. The bubble content assumed to be a mixture of non-condensable diatomic ideal gas, and glycerine vapour. Therefore the pressure inside the bubble is the sum of the partial pressures of the gas (air) p_G and vapour p_V. The pressure of gas content was approximated by an adiabatic relationship:

$$p_G=p_{G0}\left(\frac{R_0}{R}\right)^{3\kappa}. \quad (3)$$

The ratio of specific heats is $\kappa=1.4$. The mass of the gas inside the bubble are determined by the reference pressure p_{G0}, and the reference bubble radius R_0:

$$m_G=\frac{4p_{G0}R_0^3\pi}{3\Re T_\infty}, \quad (4)$$

where $\Re$ is the specific gas constant. The connection between the pressures in the liquid and the gas/vapour domain at the bubble wall, is described by the mechanical balance:

$$p_G+p_V=p_L+\frac{2\sigma}{R}+4\mu_L\frac{\dot{R}}{R}, \quad (5)$$

where σ is the surface tension and μ_L is the dynamic viscosity of the glycerine, both depend on the ambient temperature T_∞. The material properties were taken from the results of The Dow Chemical Company [14].

2.1 Reducing the number of parameters

In Eqs. (1) to (5) all parameters can be determined with five quantities [15]. The ambient pressure P_∞ and the ambient temperature T_∞ specify the material properties of a pure substances. In our special case, all material properties of glycerine depend on only the ambient temperature T_∞, the dependence of P_∞ is neglected. The equilibrium radius of the bubble was prescribed, $R_E = 0.1\ mm$, to determine the size of the bubble. For unexcited system ($p_A = 0$), and all time derivates are zeros, thus Eq. (5) can be rewritten:

$$0 = p_V - P_\infty + p_{G0}\left(\frac{R_0}{R_E}\right)^{3\kappa} - \frac{2\sigma}{R_E}. \tag{6}$$

Since the mass of the bubble depend on the product of $(p_{G0}R_0^3)$, either the reference pressure p_{G0} or the reference bubble radius R_0 can be chosen arbitrarily. In our case, the reference bubble radius was chosen to be equal to equilibrium radius R_0=R_E, thus from Eq. (6) the reference gas pressure can be calculated:

$$p_{G0} = \frac{2\sigma}{R_E} - (p_V - P_\infty). \tag{7}$$

The remaining two parameters are the pressure amplitude p_A and the angular frequency ω of the excitation, see Eq. (2). The angular frequency can vary between several orders of magnitude, therefore it was normalized with the linear eigenfrequency of the undamped system [2]:

$$\omega_0 = \sqrt{\frac{3\kappa(P_\infty - p_V)}{\rho_L R_E^2} + \frac{2(3\kappa - 1)\sigma}{\rho_L R_E^3}}. \tag{8}$$

The dimensionless relative frequency, which was used during the computations is defined as:

$$\omega_R = \frac{\omega}{\omega_0}. \tag{9}$$

The Mach number corresponding to the bubble wall velocity:

$$M = \frac{\dot{R}}{c_L}. \tag{10}$$

During the simulation, the bubble radius, the bubble wall velocity and the time was normalized with reference quantities. The reference bubble radius was the equilibrium radius $R_{ref} = R_E$, the reference velocity defined as $v_{ref} = R_E/t_{ref}$, where $t_{ref} = \omega/2\pi$.

3. PROPERTIES OF THE BUBBLE OSCILLATOR

3.1. Computation of stable solutions

The Keller—Miksis model can be viewed as a two dimensional nonlinear oscillator. Closed analytic solutions are not known, except for empty bubble [13], however, numerical solutions are easily obtained. The simplest method is to use an initial value problem solver with suitable initial conditions for the radius of the bubble $R(0)$ and for the velocity of the bubble wall $\dot{R}(0)$, then integrate the system forward in time. After some transient period, the trajectory progressively converges to a stable state, called attractor.

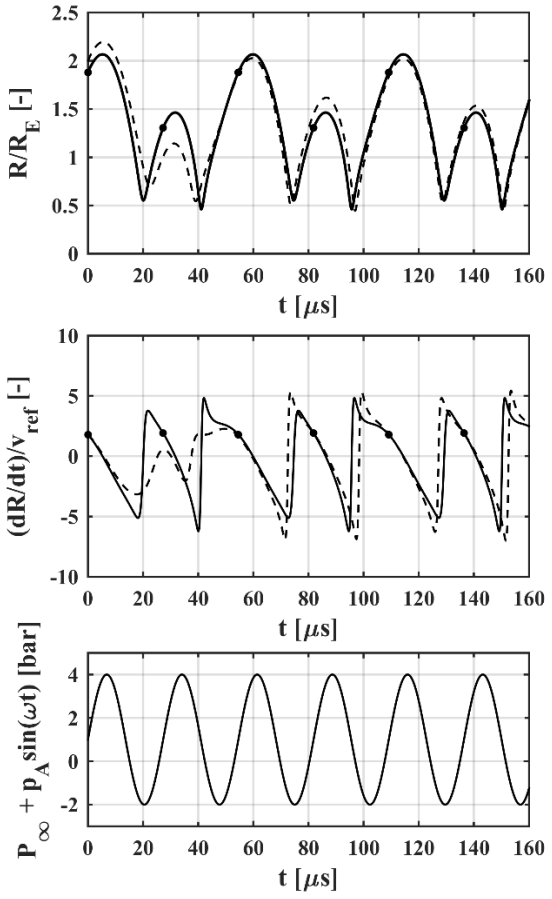

Figure 1. Dimensionless bubble radius and bubble wall velocity vs. time curves at $p_A = 4\ bar$ and $\omega_R = 1.25$. The solid line denotes the attractor, the dashed line denotes the transient solution. The lower graph represent the pressure excitation in time. The black dots are the points of the Poincaré sections.

A typical example of solution is presented in Figure 1 at $p_A = 4bar$ and $\omega_R = 1.25$. On the upper, chart, the dimensionless bubble radius R/R_E, on the middle chart the dimensionless bubble wall velocity

$\dot{R}/v_{ref}$ are presented as a function of time. The solid line denotes the attractor, and the dashed line denotes the transient solutions. The lower graph represent the harmonic pressure excitation (see Eq. (2)).

The solution can be represented in the $(R, \dot{R})$ phase plane. In the simplest case, the trajectory of an attractor construct a closed curve on the phase plane. Figure 2 shows the attractor of the solutions apparent in Fig. 1, in the phase plane. The transient trajectory (dashed curve) starts from the initial condition (denoted by empty circle) and converges to the steady state (solid cure).

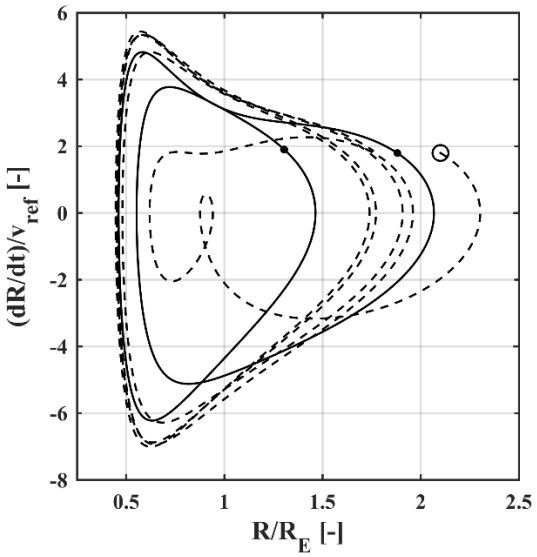

Figure 2. The normalized bubble radius–bubble wall velocity phase plane. Dots are the points of Poincaré sections, and the round denotes the initial conditions.

The trajectories of the complex solution may intersect themselves, making the representation of the results difficult. To avoid this difficulty, one can represent only the Poincaré map, obtained by sampling the continuous trajectory at every integer multiple of the period of driving time t_0. The dots in Fig. 1 and Fig. 2 are the points of Poincaré sections.

During our investigation, the whole trajectories was not recorded, only the Poincaré maps and the maximum values of bubble radius and wall velocity. With these quantities, the main characteristics of the oscillation can be described without the representation of the trajectories. The employed software was Matlab, and the numerical method was a 4th order Runge—Kutta scheme with 5th order embedded error estimation.

3.2. The different types of stable solution

Besides the the simplest solution with period t_0, sub-harmonic oscillations may occur, which only repeat after 2, 3 or more period of excitation, hence the attractor returns exactly to the starting value after 2, 3, or more acoustic cycles. If the solution return to themselves after N period of excitation, where N is integer, the solution called period N solution.

Since the solution is sampled every integer multiple of t_0 in the phase plane, the period N solutions are represented by N dots. In Figure 3, period 1 (solid line), 2 (dashed line) and 3 (dotted line) solutions are demonstrated. On the upper panel, the normalized bubble radius R/R_E as a function of normalized time $\tau = t/t_{ref}$, on the lower panel the periodic attractors in the dimensionless phase plane are represented, respectively. Observe that the solution demonstrated on Fig. 1 and Fig 2 was 2 period solution.

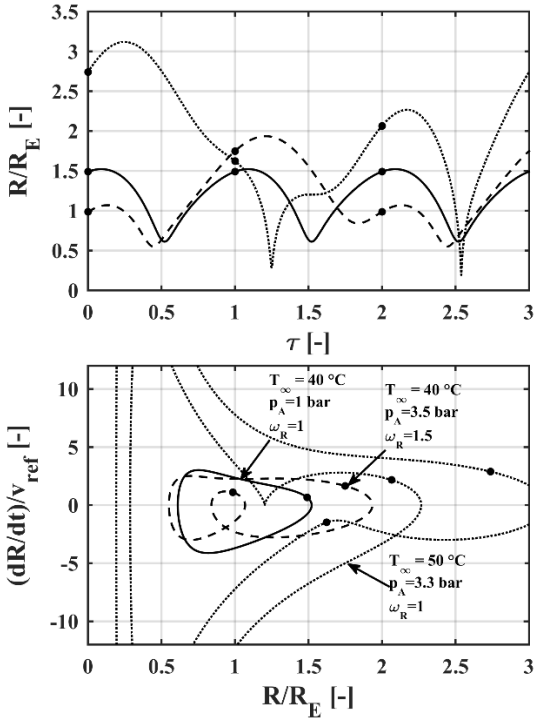

Figure 3. Examples of different periodic attractors: period 1, 2 and 3 solutions are denoted by solid, dashed and dotted lines.

The period may even go to infinity to yield never repeating bubble oscillations. In this case, trajectories never closing. This type of solution is called chaotic attractor.

An example for chaotic solution is demonstrated in Figure 4. On the phase plane (lower panel), trajectories are not plotted, only the points of Poincaré points are represented, to avoid overbidding the figure.

In Figure 5 the spectrum of the period 1, 2, 3 and chaotic solutions, which were demonstrated in Fig. 3 and Fig. 4 are represented. The frequency of the bubble oscillation f was normalized with the driving frequency ν. On subplot a) (period 1 solution), the fundamental frequency is same as the frequency of the excitation, there are peaks at $f/\nu = 1$ and at its harmonics. The spectrum on subplot b) belongs to the period 2 solution. It shows that a sub-harmonic frequency appeared at $f/\nu = 1/2$, therefore, the bubble oscillation repeat after two acoustic cycles.

On subplot c), sub-harmonics appearing at $f/\nu = 1/3$ and $f/\nu = 2/3$. This spectrum belongs to the period 3 solution. The spectrum of the chaotic solution subplot d) is continuous, where a broad band noise is superimposed on the fundamental frequency, but it's from a deterministic system.

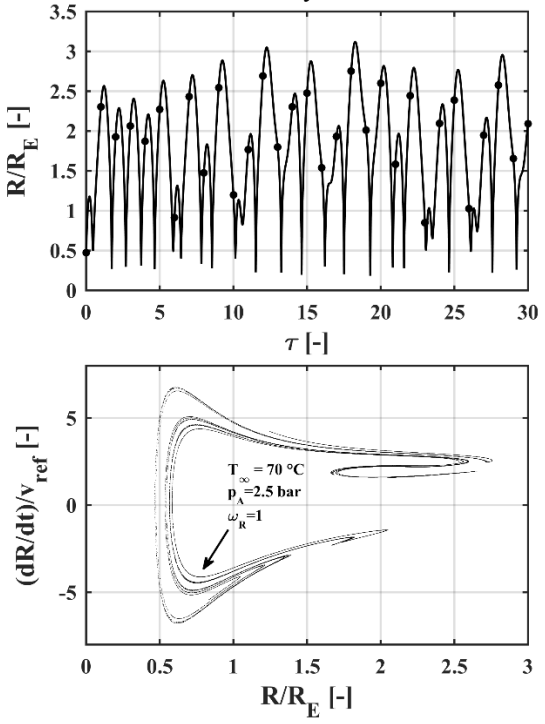

Figure 4. Example of chaotic attractor.

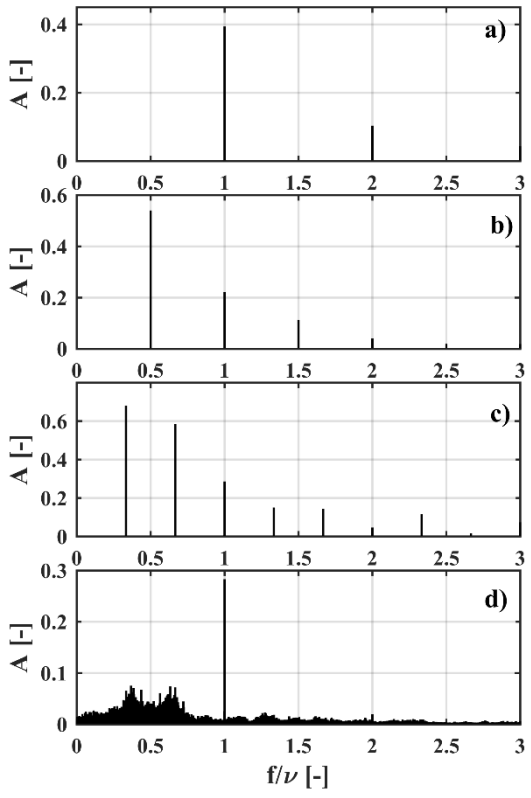

Figure 5. The spectrum of the different types of solution.

4. BIFURCATION DIAGRAMS

A usual way to investigate a periodically driven dynamic system, is to present the bifurcation diagrams. In a bifurcation diagram, only one coordinate of the Poincaré section is plotted as a function of a parameter, called "control parameter". In Figure 6, the upper chart is a pressure amplitude bifurcation diagram, in which the normalized bubble radius of the points of the Poincaré section (R_P/R_E) were plotted as a function of the pressure amplitude p_A at constant $\omega_R = 1.25$ driving frequency. During the computation, the pressure amplitude was increased by 0.01 *bar* from 0.01 to 5 *bar*. At each parameter, 5 randomly generated initial conditions were applied in the simulations to reveal the coexisting stable solutions. The period N solutions generate N points on the bifurcation diagram. If the solution was chaotic, 512 points were plotted, which appear in a scattered way along a vertical line bounded by the size of the attractor.

A period 1 solution is bifurcated from the equilibrium state of the unexcited system ($p_A = 0\ bar$ and $R_P/R_E = 1$). As the pressure amplitude increasing, the solution undergoes a period doubling sequence, then approximately at pressure amplitude $p_A = 4\ bar$ the bubble oscillation became chaotic. After a short chaotic segment, simple periodic and chaotic windows alternate. The relevant periodic solutions are marked by numbers on the diagram.

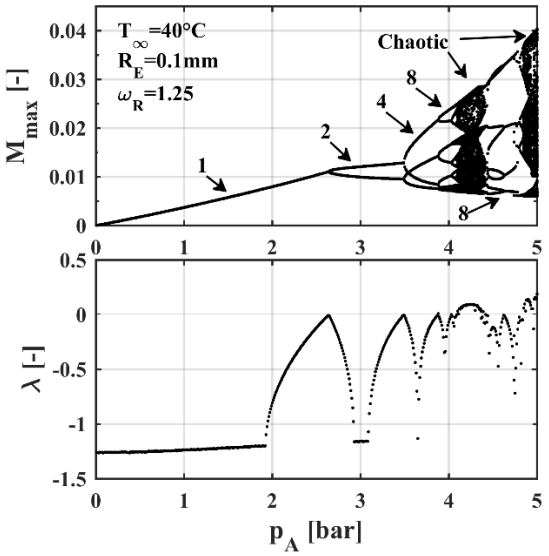

Figure 6. Pressure amplitude bifurcation diagram and Lyapunov exponent at $\omega_R = 1.25$ driving frequency

On the lower panel, the Lyapunov exponent λ (see [13], [16-17]), was plotted as a function of the pressure amplitude p_A. The Lyapunov exponent lower than zero for periodic oscillation. When the oscillation approaches a period doubling point, the Lyapunov exponent approaches zero. For chaotic solutions the Lyapunov exponent gets positive value.

Figure 7 shows similar bifurcation diagrams, but the control parameter was the relative frequency ω_R.

It increased from 0.01 to 3 with the increment of 0.01, and again 5 random initial conditions were applied to reveal the coexisting stable attractors. In this case, the pressure amplitude was chosen constant during the simulation ($p_A = 4\ bar$).

On the upper panel, the normalized bubble radius R_P/R_E versus relative frequency ω_R was plotted. The Arabic numbers mark the periodic solutions. The figure shows that there is a saddle-node bifurcation [15] at $\omega_R = 0.25$, then the period 1 solutions undergoes a period doubling sequence. Near to $\omega_R = 1$ (the frequency of the excitation equal with the eigenfrequency of the undamped system, $\nu = f_0 = 29{,}3\ kHz$) a chaotic window appeared. After the chaotic window, period halving processes can be observable. On the lower graph, the Lyapunov exponent as the function of the relative frequency was plotted, which aids to distinguish the simple periodic and chaotic solutions.

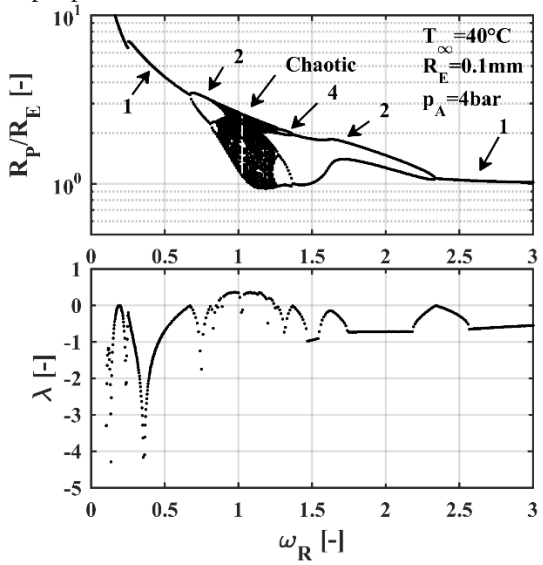

Figure 7. Frequency response curves and Lyapunov exponent at $p_A = 4\ bar$ pressure amplitude.

5. DETAILED PARAMETER STUDY

It was mentioned earlier that the oscillation of bubble depends only on five parameters. In the present investigation, the effect of the pressure amplitude p_A and the frequency ω_R were studied in detail. Further pressure amplitude bifurcation diagrams, and frequency response curves were calculated at different relative frequencies ω_R, and at different pressure amplitudes p_A. The ambient temperature $T_\infty = 40\ °C$, the ambient pressure $P_\infty = 1\ bar$ and the equilibrium radius $R_E = 0.1\ mm$ was constant during each simulation. The parameter set, which was used in the present research is summarized in Table 1.

Table 1. Parameter set during numerical computation

Equilibrium radius	R_E	0,1 [mm]
Ambient pressure	P_∞	1 [bar]
Ambient temperature	T_∞	40 [$°C$]
Relative frequency	ω_R	0-3 [-]
Pressure amplitude	p_A	0-5 [bar]

After the convergence of the solutions, the points of the Poincaré section, the maximum values (radius and wall velocity) of the oscillation, and the Lyapunov exponent were recorded. The results of the computation can be summarized on two dimensional contour plots.

Fig. 6 and Fig. 7 showed that the Lyapunov exponent helps to distinguish the simple periodic and chaotic oscillations. Figure 8 represents the values of the Lyapunov exponent λ as a function of the pressure amplitude p_A and the relative frequency ω. The diagram helps to identify the chaotic region, where the Lyapunov exponent bigger than zero (black area). It shows that the oscillation become chaotic between $\omega_R = 0.75 - 1.5$ and above $p_A = 3.5\ bar$. The white colour corresponding to the zero values of the Lyapunov exponent, where the period doubling bifurcations or the transition of periodic to chaotic solution takes place. If the Lyapunov exponent smaller than zero (grey area) the solution converges to a simple periodic attractor. The driving frequency ν is denoted on the secondary (top) x axes.

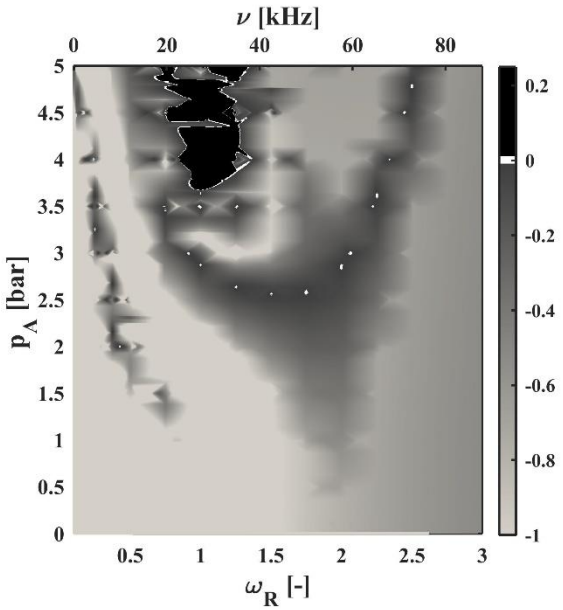

Figure 8. Lyapunov exponent λ as a function of the pressure amplitude p_A and frequency ν (or relative frequency ω_R) of excitation.

Behnia et al. [18] emphasize the importance of chaos control in medical application such as drug delivery. The oscillation of the bubble generate local turbulence and liquid microcirculation. It can be exploited in application such as micromixing and

microstreaming [19-20]. These application may operate efficiently in the chaotic region.

In order to investigate the strength of the collapse, the maximal bubble wall velocity $\dot{R}_{Max}$, rescaled to the Mach number M_{Max}, plotted on logarithmic scale in the $p_A - \omega$ parameter plane, shown in Figure 9. It shows that the at lower relative frequency, lower than $\omega_R = 0.5$, and at higher pressure amplitude, higher than $p_A = 1\,bar$, the bubble wall velocity increase rapidly (dark grey are), and reach the speed of sound, where $M_{Max} = 1$. The boundary of $M_{Max} = 1$ is marked with white colour on the contour plot. According to [13], such small frequency domain is called as "Giant response region". As the frequency is increasing and the pressure amplitude is decreasing, the available maximal Mach number is decreasing (light grey area) as well. The frequency of irradiation ν is represented on the secondary x axis as well.

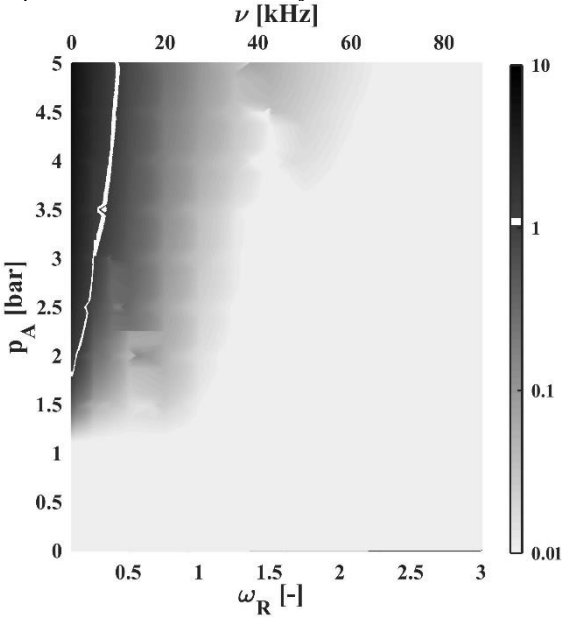

Figure 9. The maximal Mach number M_{max} on logarithmic scale as a function of the pressure amplitude p_A and relative frequency ω_R of excitation.

More violent collapse of the bubble can be reached, when the frequency of the excitation is below the main resonance. The applications may operate in an efficient way in this regions.

At higher frequencies the bubble oscillate softly, but there are application such as micromixing and microstreaming [19-20], where the oscillation of the bubble, generate local turbulence and liquid micro-circulation, which enhance the rate of the transport processes.

6. SUMMARY

The excited spherical gas/vapour bubbles behave like a nonlinear oscillator. During the oscillation of the bubble, at the collapse-phase, extreme conditions are generated such as high temperature, pressure and shock waves. These conditions are exploited in many fields of industry by the rapidly developing ultrasonic technology. This is the main motivation to investigate a spherical excited bubble placed into the highly viscous glycerine.

We seek parameter regions, where the bubble wall velocities as high as possible, may be even higher than the sound speed in the liquid domain. The high viscosity of the glycerine means high damping rate, which weakens the strength of the collapse. The applied bubble model was the modified Keller—Miksis equation, which takes into account the liquid compressibility. The two investigated parameter was the pressure amplitude p_A and the angular frequency ω of the harmonic excitation, according to the ultrasonic irradiation. The other parameters were constant during the investigation.

The results showed that at lower relative frequencies below $\omega_R = 0.5$ and higher pressure amplitude than $p_A = 1\,bar$ the bubble wall velocity reaches the sound velocity or even higher, resulting in supersonic bubble wall velocity. This region called as the giant response region. The application could operate efficiently in this parameter region.

For higher frequencies and smaller pressure amplitudes the bubble wall velocity does not reach extreme values. This domain can be important in cases, when the strong bubble collapse not a strict requirement, for example in micromixing or microstreaming.

ACKNOWLEDGEMENTS

This research has been supported by the Hungarian Scientific Research Fund – OTKA, from the grant no. K81621.

REFERENCES

[1] Koch, P., Kurz, T., Parlitz, U., Lauterborn, W., 2011, "Bubble dynamics in a standing sound field: The bubble habitat", Acoust. Soc. Am. Vol. 130, pp. 3370-3378.

[2] Brennen, C.E., 1995, "Cavitation and bubble dynamics", Oxford University Press, New York.

[3] Storey, B.D., Szeri, A.J., 2000, "Water vapour, sonaluminescence and sonochemistry", Proc. R. Soc. Lond. Vol. 456, pp. 1685-1709.

[4] Kanthale, P., Ashokkumar, M., Grieser, F., 2009, "Sonoluminescence, sonochemistry (H_2O_2 yield) and bubble dynamics: Frequency and power effects." Ultrason. Sonochem. Vol. 15, pp. 143-150.

[5] Taleyarkhan, R.P., West, C.D., Cho, J.S., Lahey, Jr.R.T., Nightmatulin, R.I., Block, R.C., 2002. "Evidence for nuclear emissions during acoustic cavitation." Science Vol. 295, pp. 1868-1873.

[6] Lahey, Jr.R.T., Taleyarkhan, R.P., Nigmatulin, R.I., 2007. “Sonofusion technology revisited.” Eng. Des. Vol. 237, pp. 1571-1585.

[7] Knorr, D., Zenker, M., Heinz, V., Lee, D-U., 2004, “Application and potential of ultrasonics in food processing.” Trends Food Sci. Tech. Vol. 15, pp. 261-266.

[8] Konaganti, V.K., Madras, G., 2010, “Ultrasonic degradation of poly(methyl metharcrylate-co-alkyl acrylate) copolymers.” Ultrason. Sonochem, Vol. 17, pp. 403-408.

[9] Rosenthal, I., Sostaric, J.Z., Riesz, P., 2004, “Sonodynamic therapy – a review of the synergistic effects of drugs and ultrasound.” Ultrason. Sonochem. Vol. 11, pp. 349-363.

[10] Hernot, S., Klibanov, A.L., 2008, ‘Microbubbles in ultrasound-triggered drug and gene delivery.” Adv. Drug. Deliv. Rev. Vol. 60, pp. 1153-1166.

[11] Yu, T., Wang, Z., Mason, T.J., 2004, “A review of research into the uses of low level ultrasound in cancer therapy.” Ultrason. Sonochem. Vol. 11, pp. 95-103.

[12] Keller, J.B., Miksis., 1980, “Bifurcation structure of the classical Morse oscillator.” J. Chem. Phys. Vol. 93, pp. 3950-3957.

[13] Lauterborn, W., Kurz, T., 2010, “Physics of bubble oscillations of gas bubbles in liquids.” J. Acoust. Soc. Am. Vol. 59, pp. 283-293.

[14] Dow Chemical Company, http://www.dow.com/

[15] Hegedűs, F., 2014, “Stable bubble oscillations beyond Blakes critical threshold.” Ultrasonics Vol. 54, pp. 1113-1121.

[16] Lauterborn, W., Parlitz, U., 1988, “Methods of chaos physics and their application to acoustics.”, J. Acoust. Soc. Am. Vol. 84, pp. 1975-1993.

[17] Parlitz, U., Englisch, V., Scheffcyk, C., Lauterbor, W., 1990, “J.Acoust. Soc. Am. Vol. 88, pp. 1061-1077.

[18] Behnia, S., Sojahrood, A. J., Soltanpoor, W., Jahanbakhsk O., 2009, “Suppressing chaotic oscillations of a spherical cavitation bubble through applying a periodic perturbation.”, Ultrason. Sonochem. Vol. 16, pp. 502-511.

[19] Nyborg, W. L., 1958, “Acoustic streaming near a boundary.” J. Acoust. Soc. Am. Vol. 30, pp. 329-339.

[20] Lighthill, S. J., 1978, “Acoustic streaming.” J. Sound Vib. Vol. 61, pp. 391-418.